

The Bologna Complete Sample of Nearby Radio Sources

G. Giovannini^{1,2}, G.B. Taylor³, L. Feretti², W.D. Cotton⁴, L. Lara^{5,6}, and T. Venturi²

giovann@ira.cnr.it, gtaylor@nrao.edu, lferetti@ira.cnr.it,
 bcotton@nrao.edu, lucas@ugr.es, tventuri@ira.cnr.it

ABSTRACT

We present a new, complete, sample of 95 radio sources selected from the B2 and 3CR catalogues, with $z < 0.1$. Since no selection effect on the core radio power, jet velocity, or source orientation is present, this sample is well suited for statistical studies. In this first paper we present the observational status of all sources on the parsec (mas) and kiloparsec (arcsec) scale; we give new parsec-scale data for 28 sources and discuss their parsec-scale properties. Combining these data with that in the literature, information on the parsec-scale morphology is available for a total of 53 radio sources with different radio power and kpc-scale morphology. We investigate their properties. We find a dramatically higher fraction of two-sided sources in comparison to previous flux limited VLBI surveys.

Subject headings: galaxies: active — galaxies: jets — galaxies: nuclei — radio continuum: galaxies

¹Dipartimento di Astronomia, Universita' di Bologna, via Ranzani 1, 40127 Bologna, Italy

²Istituto di Radioastronomia del CNR, via Gobetti 101, 40129 Bologna, Italy

³National Radio Astronomy Observatory, PO Box O, Socorro NM 87801, USA

⁴National Radio Astronomy Observatory, 520 Edgemont Rd, Charlottesville
 VA 22903-2475, USA

⁵Dpto Fisica Teorica y del Cosmos, Universidad de Granada, avda Fuentenueva s/n, 18071 Granada, Spain

⁶Instituto de Astrofisica de Andalucia, CSIC. Apdo. 3004, 18080 Granada, Spain

1. Introduction

The study of the parsec scale properties of radio galaxies is crucial to obtain information on the nature of their central engine, and provides the basis of the current *unified theories* (see e.g. Urry & Padovani 1995), which suggest that the appearance of active galactic nuclei strongly depends on orientation. In the *high-luminosity unified scheme*, quasars and powerful FR II radio galaxies should be the same class of objects seen at different viewing angles. Similarly, the *low-luminosity unified scheme* assumes BL-Lacs to be the beamed population of radio galaxies of low-intermediate luminosity (FR I).

To gain new insights in the study of radio galaxies on pc scales, it is important to select source samples from low frequency catalogues, where the source properties are dominated by the unbeamed extended emission and are not affected by observational biases related to orientation effects. To this aim, we undertook a project to observe a complete sample of radio galaxies selected from the B2 and 3CR catalogs (Giovannini et al. 1990, 2001). However, because of obvious observational limitations at the time of the sample selection, we chose radio sources with a relatively high core flux density (> 100 mJy at 6 cm). This clearly favors objects with a beamed core, i.e., oriented at a small angle with respect to the line of sight. We will refer to this sample as the *Bologna Strong Core Sample* (BSCS).

To overcome this bias, we recently selected a **second sample** with all the B2 and 3CR radio sources present in the same sky region of the first sample with $z < 0.1$, regardless of the core flux density: the *Bologna Complete Sample* (BCS). This sample consists of 95 sources and includes all the sources of the BSCS except 3C109, 3C 303, and 3C 346 because of the redshift limit. At present 53 of the 95 sources have been studied with VLBI observations. Here we present this new sample, report pc-scale data for the 53 sources with VLBI observations, and discuss in detail the structure and properties for the 28 sources with new VLBI data. In the near future we plan to observe the 42 sources not yet observed with parsec resolution using the phase-referencing technique since the nuclear flux density in these sources is too low to be detected using the standard technique.

For consistency with previous studies we adopt a Hubble constant $H_0 = 50$ km sec $^{-1}$ Mpc $^{-1}$ and $q_0 = 0.5$ ($\Omega_0 = 1$). Because of the low redshift limit the adopted value of the cosmological constant Ω is not relevant.

2. The Sample

In Table 1 we give the complete list of radio sources and summarize the most relevant information. The sample, consisting of 95 radio galaxies and BL-Lac type objects, was obtained from the B2 and 3CR catalogues. We used the sources above a homogeneous flux density limit of 0.25 Jy at 408 MHz for the B2 sources and above 10 Jy at 178 MHz for the 3CR sources (Feretti et al. 1984), and applied the following criteria:

- Declination $> 10^\circ$
- Galactic latitude $| b | > 15^\circ$
- Redshift $z < 0.1$

For all sources high quality images at arcsecond resolution obtained with the Very Large Array (VLA) of the NRAO¹ are available in the literature, allowing a detailed study of the large scale structure. According to the kpc-scale morphology the sample contains: 65 FR I radio galaxies; 15 FR II sources; 13 compact sources, and 1 FRI/II source. One more source has been tentatively classified as a spiral galaxy according to the optical and large scale radio structure. If confirmed it will not belong to the present sample. Moreover, VLA observations at 5 GHz provide a measure of the nuclear emission at arcsecond resolution which we refer to as the arcsecond core (see Giovannini et al. 1988), while we use the term VLBI core to refer to the unresolved compact component visible in the VLBI images at milliarcsecond resolution.

3. Observations

We obtained VLBA observing time at 5 GHz, in order to produce high resolution images for 28 sources of the BCS. For these observations we selected all sources with an estimated nuclear flux density high enough (~ 10 mJy or more) to allow standard VLBI observations (without phase-referencing). Sources with a lower core flux density will be observed in a second session. Observations were made with the full VLBA of the NRAO on April 4, 1997 (12 hours of observing time) and on January 22, 2000 (24 hours of observing time). Each source was observed for about 1 hour with short scans at different hour angles to ensure good uv-coverage. The observations were correlated in Socorro, NM. Postcorrelation processing used the NRAO AIPS package. All data were globally fringe fitted and self-calibrated. Final images were obtained using the AIPS and DIFMAP packages. The parameters of the observed sources are presented in Table 2. The VLBI core properties have been estimated by fitting a Gaussian to the VLBI image. The total VLBI flux is the correlated flux present on the short baselines. The noise level was estimated from the final images. The differences in measured noise properties are partially due to the two different observing sessions. Frequent observations of OQ208 were used to calibrate polarization terms. Images in polarization mode were obtained but no sources were detected. Limits on the polarized flux percentage are given in Table 2 as the ratio between 3σ level in the polarized map and the peak flux in the total intensity image.

¹The National Radio Astronomy Observatory is operated by Associated Universities, Inc., under cooperative agreement with the National Science Foundation.

4. Notes on Individual Sources

In the following, we provide short descriptions of all the sources presented in this paper, together with some information on the large scale structure. We present contour images for the resolved sources.

0106+13 – 3C33 (Figure 1): On the kpc-scale this narrow line FR II radio source shows a symmetric structure with two extended lobes and bright hot spots (Leahy and Perley 1991). The VLBI image shows nuclear emission with a flux density of ~ 10.6 mJy and two symmetric jets aligned with the kpc-scale structure. The southern jet is stronger and the brightness ratio to the counter-jet is ~ 2 at ~ 5 mas from the core and ~ 1 at 10 mas, suggesting a jet velocity decrease.

0326+39 (Figure 2): This is a symmetric FR I radio galaxy extended in the E–W direction, with the main jet on the western side (Bridle et al. 1991). In our VLBI image a dominant nuclear emission is seen with a short, faint jet on the same side as the main kpc-scale jet. A faint extension at $\lesssim 2\sigma$ level is present on the opposite side and could be a marginal detection of the counter-jet.

0844+31 – 4C31.32 (Figure 3): This is a symmetric narrow line FR II radio galaxy. At pc resolution a bright core and two-sided jets are visible. The symmetric pc-scale structure and the absence of a visible broad line region suggest that this source is at a large angle with respect to the line-of-sight. However, the core radio power is comparable to the total radio power, suggesting a moderate angle to the line-of-sight. The image from the VLA Faint Images of the Radio Sky at Twenty-cm Survey (FIRST, Becker et al. 1995) shows two extended FR I lobes at a larger distance from the core beyond the FR II type hot spot, indicating a prior phase of radio activity. This source could be classified as a re-started source, i.e., a source where the extended FR I structure is related to previous activity whereas the inner FR II structure originates from more recent core activity. This scenario explains the apparent contradiction of a core dominated source with a symmetric pc scale jet, since it is not expected for the present core radio power to correlate with the total source radio power: the present core dominance and the powerful parsec- scale structure could be related to a recent commencement of a third phase of increased activity. Multi-epoch observations could detect a possible growth of the inner jets allowing a more detailed study of this interesting source.

1003+35 – 3C236 (Figure 4): This giant radio galaxy, with its projected linear size of more than $6 h_{50}^{-1}$ Mpc, is the largest known radio galaxy. It has been studied on a vast range of angular scales and frequencies and it shows a complex central structure at arcsecond resolution (Fomalont, Brdle, & Miley 1982; Barthel et al. 1985). Using recent VLBI observations, Schilizzi et al. (2001); Taylor et al. (2001) discussed the structure of the steep spectrum core in detail and showed that this source has relativistic jets oriented in the same direction as the large scale structure with some oscillations (an “S” shaped structure is visible in the VLBA images by Taylor et al. (2001)). Its peculiar radio structure has been interpreted as evidence of re-started activity (O’Dea et al. 2001).

The parsec scale structure is clearly asymmetric. Schilizzi et al. (2001) measured a jet/cj ratio of ~ 50 at 1.6 GHz. In our 5.0 GHz images we find a ratio > 45 in the inner jet structure (within

10 mas from the core). This strong asymmetry implies a source orientation $\theta < 50^\circ$ with respect to the line of sight. Taking into account the large size of this source we will assume $\theta \sim 50^\circ$ which implies a highly relativistic jet velocity ($\gamma > 5$). Schilizzi et al. (2001) considered optical data (de Koff et al. 2000) and suggested an average radio axis for this source at $\sim 60^\circ$ with respect to the line of sight. This value is not too far from the value derived from the jet counter-jet ratio taking into account the jet oscillations visible in high resolution images (Taylor et al. 2001). In our VLBA images, despite of the limited uv coverage, the core is readily visible, as well as the one-sided NW jet, the compact NW blob, and the extended emission at ~ 100 mas from the core in the SE direction.

1037+30 (Figure not included): The VLA image shows a compact double structure $2''$ in size, but the position of the nucleus is uncertain. Our VLBI observation were pointed at the peak emission in the VLA image (Fanti et al. 1987). The source was not detected (< 2 mJy). This could be due to an incorrect core position and/or the presence of extended sub-arcsecond structure.

1040+31 (Figure 5): This source has a peculiar arcsecond scale radio morphology: it shows an extended halo with a jet connecting the core with a faint hot spot (Fanti et al. 1987). In our VLBI image a pc-scale jet is oriented at the same PA as the kpc-scale jet. A symmetric faint cj is visible ($\sim 2\sigma$ level). From the core dominance the source should be oriented in the range $40^\circ - 50^\circ$ with a high velocity jet. The symmetric pc-scale structure, if confirmed, implies an orientation of $\sim 50^\circ - 70^\circ$.

1102+30 (Figure 6): On the kpc-scale this source is a symmetric FR I radio galaxy. From the FIRST image there is a hint that the main jet is on the W side (see Fig. 6-left). At pc-scale resolution we find a core and a one-sided jet on the W side, confirming that the W jet is the approaching one. On the E side a low level emission may be present.

1116+28 (Figure 7): At arcsecond resolution this source shows a Narrow Angle Tail (NAT) structure with two symmetric jets. Our VLBA image is slightly resolved with a two-sided jet structure oriented in the same directions as the kpc-scale jets.

1204+34 (Figure 8): This FR II radio galaxy shows on the kpc-scale an 'X' shaped structure with a central core and possibly a one-sided jet to the NW (Fanti et al. 1987). Our VLBI image shows the core and a short one-sided jet at about the same PA as the kpc-scale, jet-like feature.

1316+29 – 4C29.47 (Figure 9): The pc-scale image shows a symmetric extended structure oriented East–West. The VLA image shows extended emission aligned with the pc-scale structure, however the two-sided jet emission at arcsecond resolution is in the N-S direction with a clear 'S' shaped structure and a 90° jet curvature (Fanti et al. 1987).

1321+31 – NGC5127 (Figure not included): On the kpc-scale a core and a two-sided symmetric jet is present. In our VLBA image only a faint unresolved nuclear component (3.7 mJy) is present. Xu et al. (2000) found at 1.67 GHz a two-sided jet aligned with the kpc-scale emission. On our shortest baseline a total flux density of 11 mJy is present, suggesting the presence of a

larger scale structure not visible in our images. We note that self-calibration is not reliable for this source because of the too low flux density.

1346+26 – 4C26.42 (Figure not included): This source is identified with the central cD in the cooling flow cluster A1795. In the VLA images it is a slightly extended ($20''$) with a FR I 'Z' shaped structure. Its interaction with the X-ray emitting gas visible in Chandra images has been recently discussed in detail (Fabian et al. 2001).

We marginally detect this source in our VLBI data. The structure is poorly defined, but possibly extended with a total flux density of ~ 8 mJy. The large difference between the arcsecond core flux density (53 mJy) and the flux density measured on the mas scale suggests the presence of extended emission with a complex morphology. Deeper observations and better (u,v) coverage will be necessary to properly image this source.

1350+31 – 3C293 (Figure 10): This source has been studied in detail at arcsecond and sub-arcsecond resolution (Beswick et al. 2004, and references therein). Here we present a pc-scale image of the core region where a two-sided jet structure is aligned with the sub-arcsecond scale structure. A large amount of correlated flux is present only on the shortest baseline (Y - VLBA-PT) but it is missing in our image because of the poor (u,v) coverage. The symmetric structure suggests that the present active jets are nearly in the plane of the sky. The connection with the kpc-scale structure is not clear. It could be a case of a restarted activity as argued for 0844+31, 1003+36, and 1842+45. In this case the recent emission appears to be at a different PA with respect to the older emission.

1414+11 – 3C296 (Figure 11): This symmetric FR I radio galaxy shows two-sided emission in our VLBI image as well as in the VLA images (Leahy and Perley 1991). From polarization observations (Garrington et al. 1996) the Southern lobe appears to be the more distant one (due to the Laing-Garrington effect). See also the Leahy et al. web page: <http://www.jb.man.ac.uk/atlas>). This is in agreement with the evidence that the brighter, kpc-scale jet points to the north, and with the brightness asymmetry in our VLBI image even if the low jet counter-jet ratio suggests an orientation close to the plane of the sky. A second epoch observation did not show any visible proper motion in this smooth radio jet.

1422+26 (Figure 12): This extended FR I galaxy shows at arcsecond resolution two symmetric jets oriented E-W, with the main jet on the western side. This source is very faint on the pc-scale (peak flux = 1.7 mJy/beam) and shows a possible one-sided jet at the same PA as the main kpc jet. If this structure is real the source is oriented at $\theta = 45^\circ - 50^\circ$ and $\beta > 0.95$. More observations are necessary to confirm this result.

1448+63 – 3C305 (Figure not included): This is a small FR I radio galaxy showing a 'plumed' double structure, with two faint hot-spots and symmetric jets (Heckman et al. 1982). The optical galaxy is peculiar with continuum emission on the HST scale perpendicular to the radio jet (Jackson et al. 1995). We marginally detected this FR I source with a possible extension perpendicular to the kpc-scale jet, i.e., aligned with the HST emission. The low correlated flux

requires a deeper image to properly study this source.

1502+26 – 3C310 (Figure 13): This powerful FR I radio source shows two symmetric extended lobes oriented in the N-S direction. No kpc-scale jets are visible in the available images. It was observed with a global array at 18 cm (Gizani and Garrett 2002) and a peculiar pc-scale structure was found: two compact components almost perpendicular to the extended structure and an extended emission to the north, but misaligned by about 20° with respect to the extended lobes. Our 6 cm image is inconsistent with this result since it shows a core and a one-sided jet to the South, aligned with the kpc-scale extended emission. According to observational data, if the pc-scale jets are highly relativistic ($\gamma > 3$) the source orientation is $\theta = 50^\circ - 70^\circ$.

1521+28 (Figure 14): This extended FR I source shows a well defined one-sided jet emission in VLA images (Capetti et al. 1995). The same structure is visible in our VLBA image where a short one-sided jet is found in alignment with the kpc-scale jet.

1529+24 – 3C321 (Figure not included): This Narrow Line FR II radio galaxy shows two symmetric lobes with hot spots and a faint jet in the NW direction. Only a point-like core is visible in our VLBA map. From the core dominance, we find that high velocity jets are in agreement with observational data only if θ is $45^\circ - 70^\circ$. This relatively large orientation angle is consistent with the lack of a visible broad line region.

1553+24 (Figure 15): At arcsecond resolution this source shows a well defined high brightness main jet and a faint counter-jet. An optical jet has been found coincident with the main kpc-scale jet (Capetti et al. 2000). Our mas scale image shows a one-sided jet structure aligned with the optical and large-scale jet. We derive from our data an inclination angle $\theta = 30^\circ - 40^\circ$ in agreement with the presence of an optical jet.

1557+26 – IC4587 (Figure 16): In the FIRST image there is an extended emission with a total flux density of 32.4 mJy. The host galaxy is identified as a low redshift (0.0442) elliptical galaxy (Parma et al. 1986). A nearby point-like source with a flux density of 120 mJy is present at about $30''$ east of the core. The two sources are probably unrelated therefore the radio galaxy IC4587 is below the B2 flux density limit (because the large beam in the B2 catalogue blended the two sources). The VLBA component associated with IC4587 is slightly extended in the same direction of the arcsecond structure visible in the FIRST image. The data presented here are for IC4587 only.

1613+27 (Figure not included): A typical FR I radio galaxy. In our VLBA image we detect only unresolved nuclear emission.

1621+38 – NGC6137 (Figure 17): This head-tail radio galaxy has bright, short symmetric jets oriented N-S on the kpc-scale, and an extended low brightness tail to the east (Fanti et al. 1987). In our VLBI image a bright core and a one-sided jet is present. The pc-scale jet is slightly misaligned, but oriented on the same side with respect to the core as the brighter kpc-scale jet ($\sim 160^\circ$ VLBI, $\sim 190^\circ$ VLA).

1658+30 – 4C30.31 (Figure 18): On the kpc-scale this source has a symmetric FR I morphology with two extended lobes. The main jet points to the SW and is easily visible while the counter-jet is embedded in the extended low brightness emission of the lobe (Fanti et al. 1987). On the parsec scale we detect a one-sided jet structure oriented in the same direction as the main arcsecond-scale jet.

1827+32A (Figure 19): This FR I radio galaxy has an S-shaped structure. In the VLA high resolution image (Fanti et al. 1987), the eastern jet is the main one and a faint counter-jet is also apparent. In our VLBI image we detect a core and a one-sided jet with the same orientation as the arcsecond-scale jet.

1842+45 – 3C388 (Figure 20): This source has been classified as an FR II source identified with a bright cD galaxy, but its radio morphology is quite peculiar: the eastern lobe is relaxed, while the western lobe shows extended structure beyond the hot spot (as in 0844+31), suggesting restarted activity (see Leahy et al. home page: <http://www.jb.man.ac.uk/atlas>). On the basis of the lack of depolarization asymmetry in the two lobes, Roettiger et al. (1994) suggest that this source is oriented close to the plane of the sky.

Our VLBI image shows a core and one-sided jet emission with the same orientation as the kpc-scale jet. Observational data suggest the presence of a relativistic jet oriented in the range 45° to 65° . We note that an angle of $\sim 60^\circ$ is in agreement with Roettiger et al. (1994) interpretation of the polarization data.

1855+37 (Figure not included): This low power compact source has a distorted double structure on the kiloparsec-scale. We did not detect this source in our VLBI observations pointed in between the two arcsecond lobes suggesting the identification as 1855+37 as a small symmetric source with a faint core.

2229+39 – 3C449 (Figure 21): We detected only a faint, unresolved core, in agreement with the orientation near to the plane of the sky of this well known FR I source (see Feretti et al. 1999).

5. Source Morphology

Among sources with VLBI data we have the following kpc-scale structures:

- 31 FR I radio galaxies
- 10 FR II radio galaxies
- 8 Compact sources with a flat spectrum
- 2 Bl-Lac objects, 1 Compact Symmetric Object (CSO), and 1 Compact Steep Spectrum Source (CSS).

Most of the extended FR I and FR II sources have a one-sided structure on the pc-scale (17 FR I and 5 FR II; see Table 3). We expect that sources at large angles to the line of sight, i.e. those less affected by relativistic effects, show a two-sided structure, i.e. small ratios between the jet and the counter-jet emission. We note, however, that the detection of a counter-jet may be related to the sensitivity of the map, whereas the dynamic range is not a problem in our images, as the sources are generally weak. We classify as two-sided all sources showing both a jet and a counter-jet, regardless of the value of the jet to counter-jet ratio, and of the length of the counter-jet.

The total number of sources showing a two-sided morphology is 16, corresponding to 30.2%. This percentage is higher than that found in previous samples in the literature: indeed there are 7/65 (11%) symmetric sources in the Pearson-Readhead (PR) sample (Pearson and Readhead 1988), and 19/411 (4.6%) in the combined PR and Caltech-Jodrell (CJ) samples (Taylor et al. 1994; Polatidis et al. 1995). The difference in the percentage of two-sided jet sources can be even larger if we consider that there are two separate classes of two-sided objects: CSOs and core-jets. The CSOs are not strongly dependent on orientation since most of the flux comes from the hot spots moving at 0.1 - 0.3 c. Nearly all symmetric sources in the PR and CJ sample are young CSO sources while very few of them are expected in the local ($z < 0.1$) universe. We note that in our sample there is only one CSO (4C31.04; Giroletti et al. 2003) and it was not classified a two-sided jet source. The difference between the percentage of symmetric sources in the present sample and in previous samples is naturally explained in the framework of unified scheme models by the fact that the present sources show relatively faint cores, and are therefore less affected by orientation bias. In particular, all two-sided FR II radio galaxies are Narrow Line objects confirming that Broad Line Radio Galaxies are oriented at least as close to the line-of-sight as quasars.

In a randomly oriented sample of radio galaxies, the probability that a source is at an angle between θ_1 and θ_2 with respect to the line-of-sight is:

$$P(\theta_1, \theta_2) = \cos(\theta_1) - \cos(\theta_2)$$

Thus, the percentage of FRI + FRII radio sources in the observed sample ($41/53 = 77\%$) corresponds to sources oriented at angles $> 40^\circ$. This is consistent with the fact that the observed sample is likely representative of a sample of sources at random angles to the line-of-sight.

It is difficult to estimate the expected number of sources showing two-sided structure in our sample, since the detection of both the jet and the counter-jet depends not only on the Doppler effect, but also on the sensitivity needed to detect the counter-jet. The values of the jet to counter-jet ratios R for the sources of our sample are given in Table 3. The high values derived for 0055+30 (NGC 315) and 0220+43 (3C 66B) are related to the presence of high brightness jets and very deep radio observations of these sources (Giovannini et al. 2001). In the other two-sided sources, the values of R are in the range 1 to 5. Most of the lower limits to R are much larger than 5, thus confirming that the sensitivity in our maps is generally good enough to detect as two-sided the sources at large angles to the line of sight. The sources with a two-sided structure in our sample

are about 30%. This percentage implies that sources with two-sided jets are oriented at angles $> 70^\circ$. This is consistent with a jet counter-jet ratio ≤ 5 if the jet velocity is of 0.9-0.99 c.

We note that a jet counter-jet ratio ≤ 5 in two-sided sources implies also that a counter-jet is easily detected only if the jet brightness is at the level of about 15 r.m.s. (using a map detection limit of 3 r.m.s.). We find that $\sim 37\%$ (10/27) of the FRI radio galaxies and 44% (4/9) of the FRII's are two-sided on the pc-scale. The higher fraction of symmetric sources among the FRII's could suggest that the jets in FRII's are intrinsically stronger than those in FRI's (assuming that the velocities are the same). We checked if the jet to counter-jet ratio is a function of the total or arcsecond core radio power. We did not find any correlation while as expected two sided sources are more frequently found in galaxies with a low core dominance. A more comprehensive analysis on jet to counter-jet ratio will be performed when VLBI data on the full radio galaxy sample are available.

Among the flat spectrum sources unresolved on the arcsecond scale, we find 5 sources with a one-sided jet (including 2 BL-Lacs), and 2 sources with symmetric structures. 2 other sources have not been detected, and 1 is still unresolved on the pc-scale. This large spread in pc-scale structures suggests that this population could include intermediate low power BL-Lac sources (one-sided), where relativistic effects are important, as well as low-power sources whose intrinsically small size might be related to a dense ISM and/or weak nuclear activity, unable to power relativistic jets out to kpc-scales.

In most sources we find a good agreement between the pc and kpc-scale structures. The comparison between the VLA and VLBA jet Position Angle (PA - see Table 3) shows that only one source (1316+29) has a $\sim 90^\circ$ misalignment, while 2 other sources (1316+29; 1621+38) have a difference of 50° and 30° respectively. This result supports the model where the large distortions detected in BL-Lac sources are due to small intrinsic bends amplified by the small angle of the BL-Lac jets to the line-of-sight. In all sources with the same jet PA in the pc and kpc scale structure, the one sided pc scale jet (or the brighter jet in double-sided pc scale jets) is oriented with respect to the nuclear emission, on the same side of the brighter kpc scale jet (main jet) confirming the presence of a continuous emission and not of a *flip-flop* jet emission. Moreover this result suggests that the presence of a small jet asymmetry in the kpc scale images could be due to Doppler boosting.

We have compared the correlated flux on the shortest VLBA baselines with the core arcsecond flux density (Table 3). In 5 sources this comparison was not possible because flux density variability or to the presence of compact steep spectrum structures; among the remaining 48 sources, 34 (70%) have a correlated flux density larger than 70% of the arcsecond core flux density. Therefore in these sources we have mapped most of the small scale structure and we are able to properly connect the pc to the kpc structures. Finally for 14 (30%) sources we are missing a significant fraction of the arcsecond core flux density (larger than 90% in a few cases) in the VLBA images. This result suggests the presence of significant structures between ~ 30 mas and 1 arcsecond where VLBA can

miss structures because of the lack of short baselines and the VLA present angular resolution can be too low. To properly study these structures future observations with the EVLA, the proposed New Mexico Array (EVLA phase 2) or the e-MERLIN array will be necessary.

6. Conclusions

In this paper we introduce a new complete sample of radio sources selected from the B2 and 3CR catalogues, with $z < 0.1$. For 53 of 95 sources we present VLBI data (28 of them for the first time) and briefly discuss the pc and kpc-scale structure.

As expected, on the parsec scale a one-sided jet morphology is the predominant structure present in our images, however $\sim 30\%$ of sources observed so far show evidence of a two-sided structure which has been quite rare in observations of sources observed to have high power cores. This result is in agreement with a random orientation of radio galaxies and a high jet velocity ($\beta \sim 0.9$).

With very few exceptions, the parsec and kpc-scale radio structures are aligned confirming that the large bends present in some BL-Lac sources are amplified by the small jet orientation angle with respect to the line-of-sight. In sources with aligned pc and kpc scale structure the main jet is always on the same side with respect to the nuclear emission.

In the majority of the sources ($\sim 70\%$) there is a good agreement between the arcsecond scale and the VLBI core flux density. However for the remaining 30% of the sources the correlated VLBI flux density is lower than 70% of the arcsecond core flux density at the same frequency. This suggests the presence of a sub-kpc-scale structure which will be best imaged with a new array such as the New Mexico Array.

No polarized flux has been detected confirming the low level of polarized emission in radio galaxies at pc resolution as found by Pollack et al. (2003).

A more detailed discussion on the properties of radio galaxies on the pc-scale, such as jet intrinsic parameters, will be presented in a future paper when data on the whole sample will be available.

We thank the referee for useful comments. This work has received partial support by the Ministero dell’Istruzione, dell’Università e della Ricerca (MIUR - Italy) under contract n. 2003027534.

REFERENCES

Barthel P.D., Schilizzi R.T., Miley G.K., Jagers W.J., Strom R.G., 1985 *A&A*148, 243

Becker R.H., White R.L., Helfand D.J., 1995, *ApJ* 450, 559

Beswick R.J., Peck A.B., Taylor G.B., Giovannini G., 2004, *MNRAS*, in press, astro-ph/0404295

Bridle A. H., Baum S. A., Fomalont E. B., Parma P., Fanti R., Ekers R. D., 1991, *A&A*245, 371

Capetti A., Fanti R., Parma P., 1995, *A&A*300, 643

Capetti A., de Ruiter H. R., Fanti R., Morganti R., Parma P., Ulrich M.-H., 2000, *A&A*362, 871

Fabian A. C., Sanders J. S., Ettori S., Taylor G. B., Allen S. W., Crawford C. S., Iwasawa K., Johnstone R. M., 2001, *MNRAS*321, L33

Fanti C., Fanti R., de Ruiter H.R., Parma P., 1987, *A&AS*69, 57

Feretti L., Giovannini G., Gregorini L., Parma P., Zamorani G., 1984, *A&A*139, 55

Feretti L., Perley R., Giovannini G., Andernach H., 1999, *A&A*341, 29

Fomalont E.B., Bridle A.H., & Miley G.K. 1982, IAU Symp. 97: Extragalactic Radio Sources, 97, 173

Garrington S.T., Holmes C.F., Saikia D.J., 1996, 175th Symposium of the International Astronomical Union, edited by R.D. Ekers, C. Fanti, and L. Padrielli, Kluwer Academic Publishers, p. 397

Giovannini G., Feretti L., Gregorini L., Parma P., 1988, *A&A*199, 73

Giovannini G., Feretti L., Comoretto G., 1990, *ApJ*358, 159

Giovannini G., et al. 1990, *ApJ*358, 159

Giovannini G., Cotton W. D., Feretti L., Lara L., Venturi T., 2001, *ApJ*552, 508

Giroletti M., Giovannini G., Taylor G.B., Conway J.E., Lara L., Venturi T. 2003, *å*399, 889

Gizani N. A. B., Garrett M. A., 2002, Proceedings of the 6th European VLBI Network Symposium, edited by E. Ros, R.W. Porcas, A.P Lobanov and J.A. Zensus, p. 159

Heckman T. M., Miley G. K., Balick B., van Breugel W. J. M., Butcher H. R. 1982, *ApJ*262, 529

De Koff S., Best P., Baum S.A., Sparks W.R., Roettgering H., Miley G., Golombek D., Macchetto F., Martel A., 2000, *ApJS*129, 33

Jackson N., Sparks W. B., Miley G. K., Macchetto F., 1995, *A&A*296, 339

Leahy J.P., Perley R.A., 1991, AJ102, 537

O'Dea C.P., Koekemoer A.M., Baum S.A., Sparks W.B., Martel A.R., Allen M.G., Macchetto F.D., Miley G.K., 2001, AJ121, 1915

Parma P., de Ruiter H. R., Fanti C., Fanti R., 1986, Astron. Astrophys. Suppl. 64, 135

Pearson T. J., Readhead A. C. S., 1988, ApJ328, 114

Polatidis A. G., Wilkinson P. N., Xu W., Readhead A. C. S., Pearson T. J., Taylor G. B., Vermeulen R. C., 1995, ApJS98, 1

Pollack L.K., Taylor G.B., Zavala R.T., 2003, ApJ589, 733

Roettiger K., Burns J.O., Clarke D.A., Christiansen W.A., 1994, ApJ421 L23

Schilizzi R. T., Tian W. W., Conway J. E., Nan R., Miley G. K., Barthel P. D., Normandea M., Dallacasa D., Gurvits L. I., 2001, A&A368, 398

Taylor G. B., Vermeulen R. C., Pearson T. J., Readhead A. C. S., Henstock D. R., Browne I. W. A., Wilkinson P. N., 1994, ApJS95, 345

Taylor G. B., Hough D. H., Venturi T., 2001, ApJ559, 703

Urry C.M., Padovani P. 1995, PASP, 107, 803

Xu C., Baum S.A., O'Dea C.P., Wrobel J. M., Condon J. J., 2000, AJ120, 2950

Table 1. The Complete Bologna Sample

Name IAU	Name other	z	Morphology	$S_c(5.0)$ mJy	$\log P_c$ W/Hz	$\log P_t$ W/Hz	Notes
			kpc				
0034+25	UGC367	0.0321	FR I	10	22.65	24.08	no VLBI
0055+26	N326	0.0472	FR I	8	22.89	25.68	no VLBI
0055+30	N315	0.0167	FR I	588	23.85	24.56	BSCS
0104+32	3C31	0.0169	FR I	92	23.06	25.11	BSCS
0106+13	3C33	0.0595	FR II	24	23.58	26.69	*
0116+31	4C31.04	0.0592	CSO	32	23.70	25.71	BSCS
0120+33	N507	0.0164	FR I	1.4	21.21	23.91	no VLBI
0149+35	N708	0.0160	FR I	5	21.74	23.60	no VLBI
0206+35	4C35.03	0.0375	FR I	106	23.82	25.46	BSCS
0220+43	3C66B	0.0215	FR I	182	23.56	25.59	BSCS
0222+36		0.0327	C	140	23.76	24.20	BSCS
0258+35	N1167	0.0160	CSS	<243	<23.43	24.65	BSCS
0300+16	3C76.1	0.0328	FR I	10	22.67	25.38	no VLBI
0326+39		0.0243	FR I	78	23.30	24.69	*
0331+39	4C39.12	0.0202	C	149	23.42	24.49	BSCS
0356+10	3C98	0.0306	FR II	9	22.57	26.01	no VLBI
0648+27		0.0409	C	213	24.19	24.31	BSCS
0708+32		0.0672	FR I	15	23.48	24.76	no VLBI
0722+30		0.0191	Spiral?	51	22.39	24.42	no VLBI
0755+37	N2484	0.0413	FR I	195	24.16	25.65	BSCS
0800+24		0.0433	FR I	3	22.39	24.42	no VLBI
0802+24	3C192	0.0597	FR II	8	22.98	26.28	no VLBI
0828+32AB	4C32.15	0.0507	FR II	3.3	22.57	25.69	no VLBI
0836+29-II	4C29.30	0.0790	FR I	131	24.63	25.70	BSCS
0836+29-I	4C29.30	0.0650	FR I	8.2	23.19	25.47	no VLBI
0838+32	4C32.26	0.0680	FR I	7.5	23.19	25.60	no VLBI
0844+31	IC2402	0.0675	FR II	40	23.91	25.88	* (1)
0913+38		0.0711	FR I	<1.0	<22.35	25.27	no VLBI
0915+32		0.0620	FR I	8.0	23.13	24.90	no VLBI
0924+30		0.0266	FR I	<0.4	<21.09	24.73	no VLBI
1003+35	3C236	0.0989	FR II	400	25.25	26.43	* (1)
1037+30	4C30.19	0.0909	C	<84	<24.49	25.63	*
1040+31		0.0360	C	55	23.49	24.98	*
1101+38	Mkn 421	0.0300	BL Lac	640	24.40	24.66	BSCS
1102+30		0.0720	FR I	26	23.78	25.35	*
1113+29	4C29.41	0.0489	FR I	41	23.64	25.12	no VLBI
1116+28		0.0667	FR I	30	23.77	25.33	*

Table 1—Continued

Name IAU	Name other	z	Morphology	$S_c(5.0)$ kpc	Log P_c mJy	Log P_t W/Hz	Notes
1122+39	N3665	0.0067	FR I	6	21.07	22.75	no VLBI
1142+20	3C264	0.0206	FR I	200	23.57	25.46	BSCS
1144+35		0.0630	FR I	250	24.90	24.95	BSCS
1204+24		0.0769	FR I	8	23.32	24.85	no VLBI
1204+34		0.0788	FR II?	23	23.80	25.45	*
1217+29	N4278	0.0021	C	<350	<21.08	21.44	BSCS
1222+13	3C272.1	0.0037	FR I	180	22.03	23.27	BSCS
1228+12	3C274	0.0037	FR I	4000	23.37	25.07	BSCS
1243+26B		0.0891	FR I	<1.8	<22.81	25.50	no VLBI
1251+27	3C277.3	0.0857	FR II	12	23.60	26.32	no VLBI
1254+27	N4839	0.0246	FR I	1.5	21.60	23.74	no VLBI
1256+28	N4869	0.0224	FR I	2.0	21.64	24.50	no VLBI
1257+28	N4874	0.0239	FR I	1.1	21.44	24.09	no VLBI
1316+29	4C29.47	0.0728	FR I	31	23.86	25.87	*
1319+42	3C285	0.0797	FR I/II	6	23.23	26.20	no VLBI
1321+31	N5127	0.0161	FR I	21	22.37	24.61	*
1322+36	N5141	0.0175	FR I	150	23.30	24.36	BSCS
1339+26		0.0722	FR I	<55	<22.11	25.47	no VLBI
1346+26	4C26.42	0.0633	FR I	53	23.97	25.75	*
1347+28		0.0724	FR I	4.8	23.05	25.08	no VLBI
1350+31	3C293	0.0452	FR I	<100	<23.95	25.96	*(1)
1357+28		0.0629	FR I	6.2	23.04	25.08	no VLBI
1414+11	3C296	0.0237	FR I	77	23.27	25.22	*
1422+26		0.0370	FR I	25.0	23.18	25.08	*
1430+25		0.0813	FR I	<1.0	<22.47	25.61	no VLBI
1441+26		0.0621	FR I	<0.7	<22.08	25.05	no VLBI
1448+63	3C305	0.0410	FR I	29	23.33	25.73	*
1502+26	3C310	0.0540	FR I	80	24.01	26.48	*
1512+30		0.0931	CSO?	<0.4	<22.19	25.02	no VLBI
1521+28		0.0825	FR I	40	24.09	25.68	*
1525+29		0.0653	FR I	2.5	22.68	24.91	no VLBI
1528+29		0.0843	FR I	4.5	23.16	25.37	no VLBI
1529+24	3C321	0.0960	FR II	30	24.10	26.47	*
1549+20	3C326	0.0895	FR II	3.5	23.10	26.54	no VLBI
1553+24		0.0426	FR I	40	23.50	24.20	*
1557+26	IC4587	0.0442	C	31	23.43	23.82	*
1610+29	N6086	0.0313	FR I	<6.0	<22.41	24.14	no VLBI

Table 1—Continued

Name IAU	Name other	z	Morphology kpc	$S_c(5.0)$ mJy	Log P_c W/Hz	Log P_t W/Hz	Notes
1613+27		0.0647	FR I	25	23.67	24.77	*
1615+35	N6107	0.0296	FR I	28	23.03	25.31	no VLBI
1621+38	N6137	0.0310	FR I	50	23.32	24.59	*
1626+39	3C338	0.0303	FR I	105	23.62	25.86	BSCS
1637+29		0.0875	FR I	13	23.65	25.44	no VLBI
1652+39	Mkn 501	0.0337	BLLac	1250	24.79	24.96	BSCS
1657+32A		0.0631	FR I	2.5	22.64	25.34	no VLBI
1658+30	4C30.31	0.0351	FR I	84	23.66	24.92	*
1736+32		0.0741	FR I	8	23.29	25.17	no VLBI
1752+32B		0.0449	FR I	12	23.03	24.45	no VLBI
1827+32A		0.0659	FR I	26	23.70	25.15	*
1833+32	3C382	0.0586	FR II	188	24.46	26.31	BSCS
1842+45	3C388	0.0917	FR II	62	24.37	26.74	*(1)
1845+79	3C390.3	0.0569	FR II	330	24.67	26.58	BSCS
1855+37		0.0552	C	<100	<24.13	25.03	*
2116+26	N7052	0.0164	FR I	47	22.74	23.57	Xu et al.(2000)
2212+13	3C442	0.0262	FR I?	2.0	21.76	25.50	no VLBI
2229+39	3C449	0.0181	FR I	37	22.72	24.96	*
2236+35		0.0277	FR I	8.0	22.43	24.41	no VLBI
2243+39	3C452	0.0811	FR II	130	24.58	26.92	BSCS
2335+26	3C465	0.0301	FR I	270	23.99	25.91	BSCS

Note. — $S_c(5.0)$ is the arc-second core flux density at 5.0 GHz and Log P_c is the corresponding logarithm of the radio power; Log P_t is the logarithm of the total radio power at 408 MHz; Morphology: C = flat spectrum compact core, CSO = Compact Symmetric Object, CSS = Compact Steep Spectrum source, FR-I or II = Fanaroff type I or II; Notes refer to the status of VLBI observations: BSCS = see Giovannini et al. 2001; * new data are given in this paper; (1) = re-started source. For a reference to the extended structure see Fanti et al. 1987 for B2 sources and Leahy et al. HTML page: <http://www.jb.man.ac.uk/atlas>).

Table 2. Observed Source Parameters

Name IAU	Name other	S_c (5.0) mJy	S_{VLBI} (tot) mJy	S_{VLBI} (core) mJy	HPBW mas	Noise mJy/beam	Polarization %
0106+13	3C33	24	30	11.0	3.5×1.4 (-5)	0.12	< 3.0
0326+39		78	74	55.5	2.8×1.6 (11)	0.14	< 1.5
0844+31	IC2402	40	32	27.0	3.4×2.0 (19)	0.08	< 1.5
1003+35	3C236	400	466	152.8	2.9×2.0 (25)	0.10	< 0.2
1037+30		< 84	< 2	N.D.	3.4×2.0 (15)	0.15	-
1040+31		55	48	37.6	2.7×2.1 (23)	0.17	< 1.0
1102+30		10	17	14.3	2.5×1.6 (-6)	0.14	< 2.5
1116+28		30	11	9.2	2.9×1.7 (-5)	0.14	< 3.5
1204+34		23	39	33.7	2.7×1.7 (-3)	0.16	< 1.0
1316+29	4C29.47	31	23	5.3	2.5×2.5	0.09	< 6.0
1321+31	N5127	21	11	3.7	2.8×1.7 (-7)	0.12	< 10.0
1346+26	4C26.42	53	8	5.8	3×3	0.10	< 5.0
1350+31	3C293	100	23	14.4	3×2.5 (0)	0.10	< 2.0
1414+11	3C296	77	86	65.1	3.6×1.7 (-4)	0.09	< 0.4
1422+26		25	3	1.7	3.5×2.0 (-2)	0.05	-
1448+63	3C305	29	2	1.1	3.6×2.0 (-5)	0.06	-
1502+26	3C310	88	3	2.7	3.6×2.2 (-3)	0.06	-
1521+28		56	44	39.5	2.9×1.6 (1)	0.04	< 0.3
1529+24	3C321	30	3	3.4	3.5×2.1 (3)	0.05	-
1553+24		40	46	40.7	3.5×1.9 (-1)	0.05	< 0.4
1557+26	IC4587	31	9	7.8	3.2×1.6 (-19)	0.26	< 10.0
1613+27		25	8	6.8	3.2×1.6 (-19)	0.24	-
1621+38	N6137	50	20	12.9	3.0×1.6 (-24)	0.11	< 2.5
1658+30	4C30.31	84	76	60.0	3.2×1.5 (-17)	0.14	< 0.7
1827+32A		26	15	5.9	2.9×1.7 (-25)	0.12	< 10.0
1842+45	3C388	62	52	34.0	2.6×1.7 (-27)	0.15	< 1.0
1855+37		<34	<2	N.D.	3.0×1.5 (-25)	0.11	-
2229+39	3C449	37	30	25.9	3.0×1.9 (-23)	0.12	< 1.5

Note. — S_c is the arcsecond core flux density at 5 GHz; S_{VLBI} (tot) is the VLBI correlated flux in the shortest baselines; S_{VLBI} (core) is the nuclear source flux density in the VLBI images.

Table 3. Parsec and Kiloparsec-scale Comparison

Name IAU	Name other	Morphology kpc	j/cj ratio	Morphology pc	S_{VLBI}/S_{VLA} %	ΔPA degree
0055+30	N315	FR I	42	2s	60	0
0104+32	3C31	FR I	>16	1s	100	5
0106+13	3C33	FR II	2.0	2s	100	0
0116+31	4C31.04	CSO	-	CSO	100	0
0206+35	4C35.03	FR I	>14	1s	80	0
0220+43	3C66B	FR I	10	2s	100	0
0222+36		C	-	C	100	0
0258+35	N1167	CSS	-	CSS	?	?
0326+39		FR I	>25	1s	100	0
0331+39	4C39.12	C	>12	1s	74	0
0648+27		C	>7.5	1s	85	-
0755+37	N2484	FR I	>20	1s	100	0
0836+29-II	4C29.3	FR I	>20	1s	100	0
0844+31	IC2402	FR II	1.0	2s	80	0
1003+35	3C236	FR II	>45	1s	100	0
1037+30	4C30.19	C	-	ND	-	-
1040+31		C	5	2s	80	0
1101+38	Mkn 421	C	>110	1s	70	0
1102+30		FR I	~1.7?	2s?	100	0
1116+28		FR I	3.3	2s	40	0
1142+20	3C264	FR I	>24	1s	60	0
1144+35		FR I	see note	2s	-	0
1204+34		FR II	>2.0	1s	100	0
1217+29	N4278	C	2.3	2s	100	-
1222+13	3C272.1	FR I	>10	1s	70	0
1228+12	3C274	FR I	>150	1s	25	0
1316+29	4C29.47	FR I	1.0	2s	70	50
1321+31	N5127	FR I	1?	2s?	50	0
1322+36	N5141	FR I	>20	1s	40	0
1346+26	4C26.42	FR I	-	C?	15	-
1350+31	3C293	FR II	2.0	2s	20	0
1414+11	3C296	FR I	2.0	2s	100	0
1422+26		FR I	>20?	1s?	10	0
1448+63	3C305	FR I	-	C?	7	90
1502+26	3C310	FR I	>2.0	1s	5	0
1521+28		FR I	>17	1s	80	0
1529+24	3C321	FR II	-	C	10	-

Table 3—Continued

Name IAU	Name other	Morphology kpc	j/cj ratio	Morphology pc	S_{VLBI}/S_{VLA} %	ΔPA degree
1553+24		FR I	>20	1s	100	0
1557+26	IC4587	C	> 4	1s	30	-
1613+27		FR I	-	C	30	-
1621+38	N6137	FR I	> 5	1s	40	30
1626+39	3C338	FR I	1.1	2s	-	0
1652+39	Mkn 501	BLLac	>1250	1s	80	-
1658+30	4C30.31	FR I	>8.5	1s	90	0
1827+32A		FR I	>7.5	1s	60	0
1833+32	3C382	FR II	>20	1s	70	0
1842+45	3C388	FR II	>10	1s	80	0
1845+79	3C390.3	FR II	>100	1s	?	0
1855+37		C	-	ND	-	-
2116+26	N7052	FR I	1.0?	2s?	-	0
2229+39	3C449	FR I	-	C	80	-
2243+39	3C452	FR II	1.1	2s	100	15
2335+26	3C465	FR I	>10	1s	100	0

Note. — 1144+35 is a two-sided source with a large flux density variability in the jet structure, see Giovannini et al. (1999). In col. 6 is given the ratio between the arcsecond core flux density and the VLBA correlated flux (at 5 GHz). ΔPA (col. 7) is the difference between the kpc and pc scale jet PA

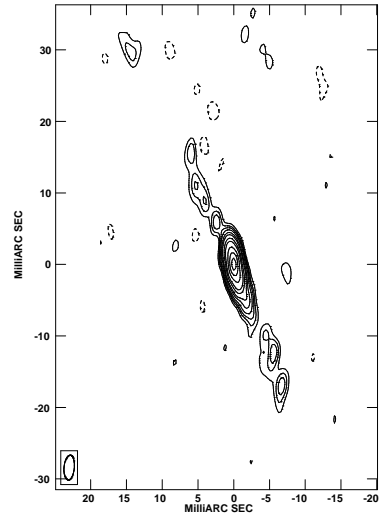


Fig. 1.— VLBA image of the narrow line FR II galaxy 0106+13 (3C33), at 5 GHz. Levs are: $-0.3, 0.3, 0.5, 0.7, 1, 1.5, 2, 3, 4, 6, 8, 10$ mJy/beam. The restoring beams of the images presented in this figure and in the following figures are given in Tab. 2

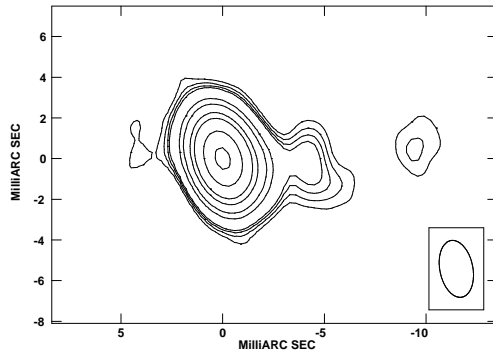


Fig. 2.— VLBA image at 5 GHz of 0326+39. Levs are: $-0.4, 0.4, 0.6, 0.8, 1, 3, 5, 10, 15, 30, 50$ mJy/beam

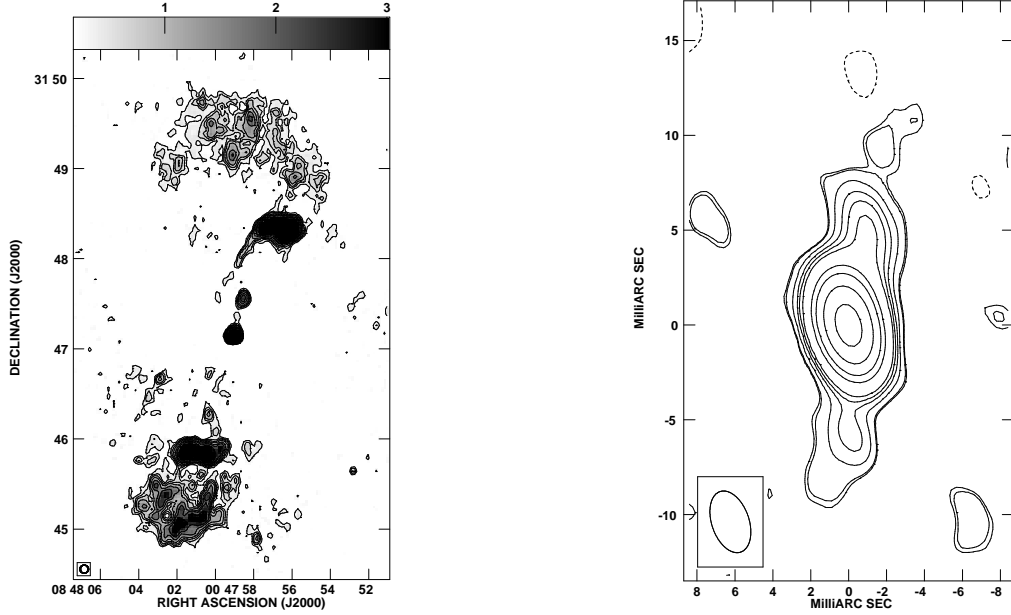


Fig. 3.— VLA image from the FIRST survey (left) of 0844+31 (IC2402) with $\text{levs} = 0.3\ 0.5\ 0.7\ 1\ 1.5\ 2\ 3\ 5\ 7\ 10\ 20\ 30\ \text{mJy/beam}$ (the HPBW is $5''$). VLBA image at 5 GHz of 0844+31 (right); levs are: $-0.15\ 0.13\ 0.15\ 0.3\ 0.5\ 0.7\ 1\ 3\ 5\ 10\ 20\ \text{mJy/beam}$.

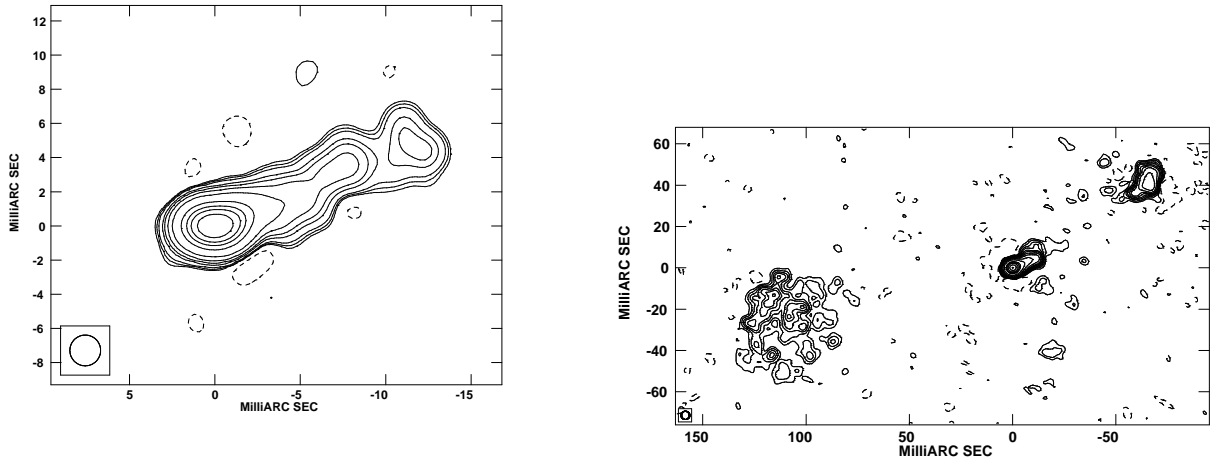


Fig. 4.— VLBA image at 5 GHz of 1003+35 (3C236) at high (left) and low resolution (right. Levs are: $-0.5\ 0.5\ 0.7\ 1\ 2\ 3\ 5\ 10\ 30\ 50\ 70\ 100\ \text{mJy/beam}$ (left) and $-0.2\ 0.2\ 0.4\ 0.7\ 1\ 1.5\ 2\ 3\ 5\ 10\ 20\ 50\ 70\ 100\ 150\ 200\ \text{mJy/beam}$ (right)).

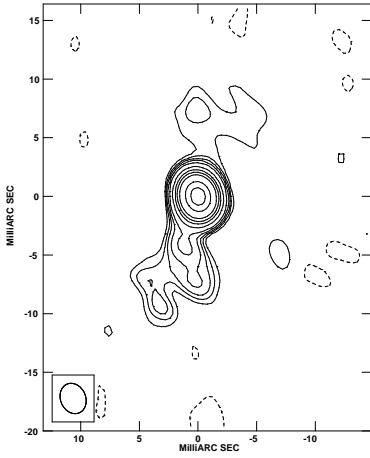


Fig. 5.— VLBA image at 5 GHz of 1040+31. Levs are: $-0.3\ 0.3\ 0.5\ 0.7\ 1\ 1.5\ 3\ 5\ 7\ 10\ 20\ 30$ mJy/beam.

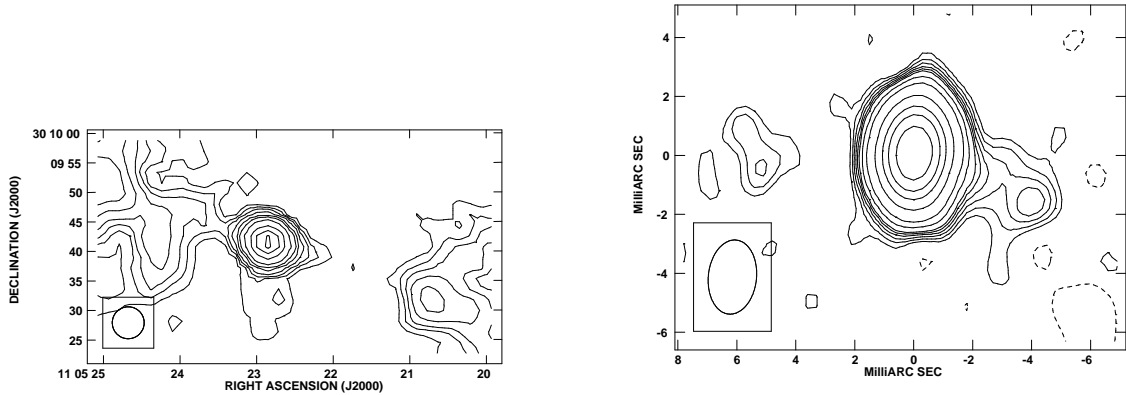


Fig. 6.— VLA image from the FIRST survey (left) of 1102+30, with $5''$ resolution. Only the innermost source region is displayed to show the direction of the main jet (West) at the arcsecond resolution. Levs are $0.3\ 0.5\ 0.7\ 1\ 1.5\ 2\ 3\ 5\ 7\ 9$ mJy/beam; VLBA image at 5 GHz of 1102+30 (right) with Levs = $-0.2\ 0.2\ 0.3\ 0.4\ 0.5\ 0.6\ 0.7\ 1\ 1.5\ 3\ 5\ 7\ 10$ mJy/beam.

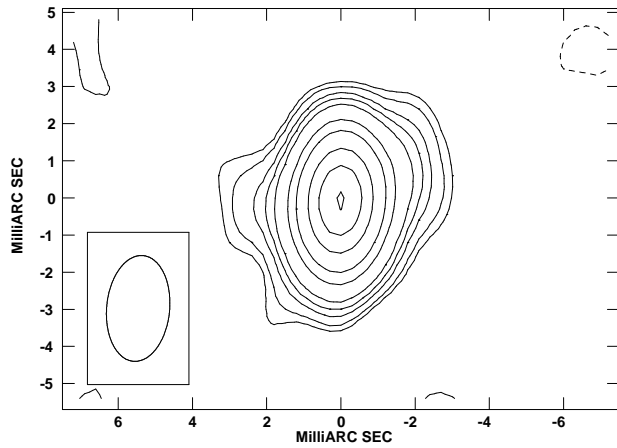


Fig. 7.— VLBA image at 5 GHz of 1116+28. Levs are: $-0.3\ 0.2\ 0.3\ 0.5\ 0.7\ 1\ 2\ 3\ 5\ 7\ 9$ mJy/beam.

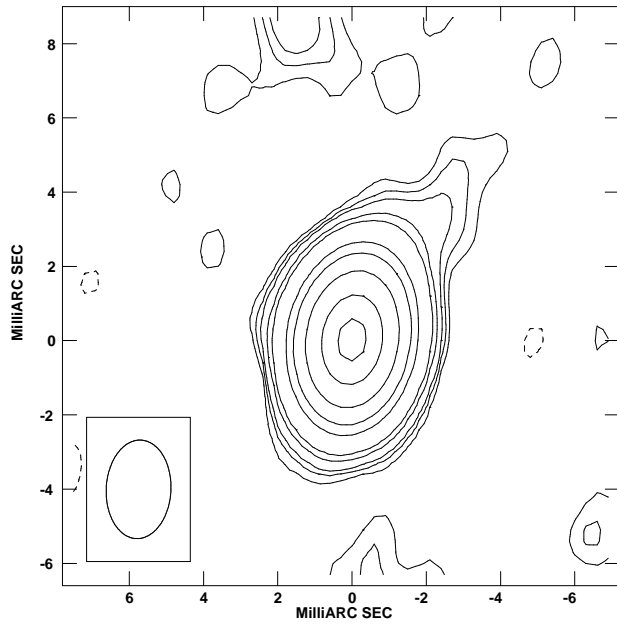


Fig. 8.— VLBA image at 5 GHz of 1204+34. Levs are: $-0.3\ 0.2\ 0.3\ 0.4\ 0.7\ 1\ 3\ 5\ 10\ 20\ 30$ mJy/beam

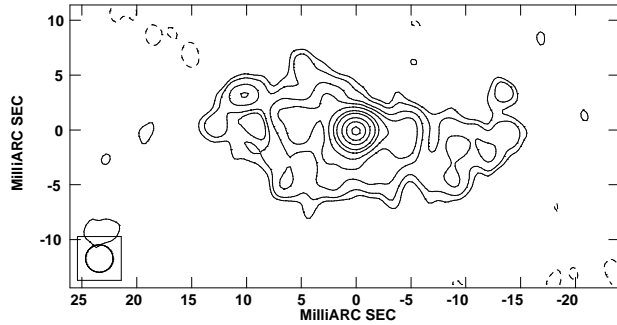


Fig. 9.— VLBA image at 5 GHz of 1316+29 (4C29.47). Levs are: -0.2 0.2 0.3 0.5 0.7 1 1.5 2 3 4 5 mJy/beam.

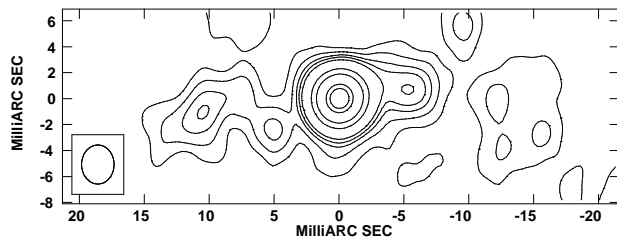


Fig. 10.— VLBA image at 5 GHz of 1350+31 (3C 293). Levs are: -0.15 0.15 0.3 0.5 0.7 1 3 5 10 12 mJy/beam.

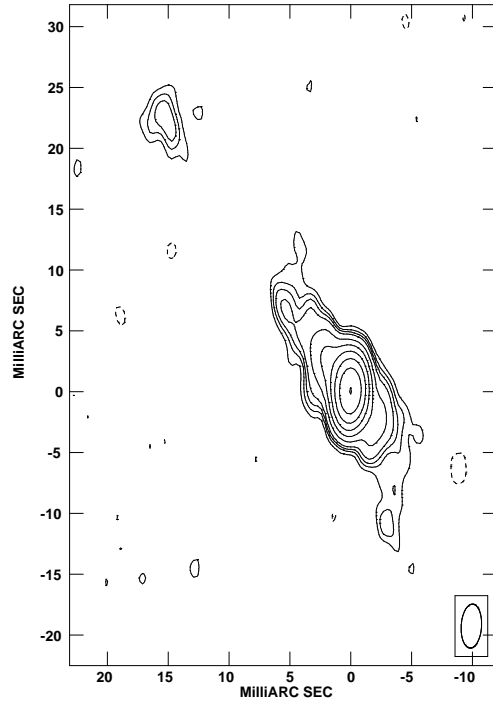


Fig. 11.— VLBA image at 5 GHz of 1414+11 (3C 296). Levs are: -0.3 0.3 0.5 0.7 1 2 4 8 16 32 64 mJy/beam.

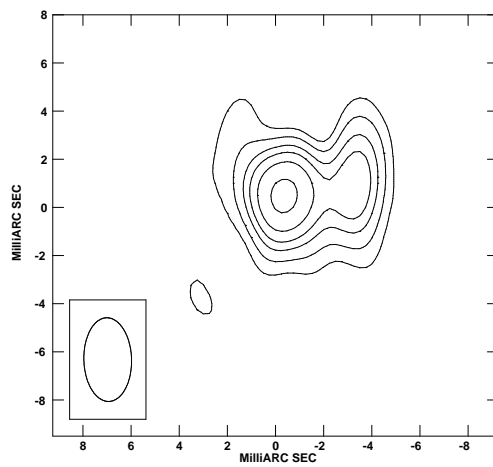


Fig. 12.— VLBA image at 5 GHz of 1422+26. Levs are: -0.15 0.15 0.3 0.5 0.7 1.5 mJy/beam

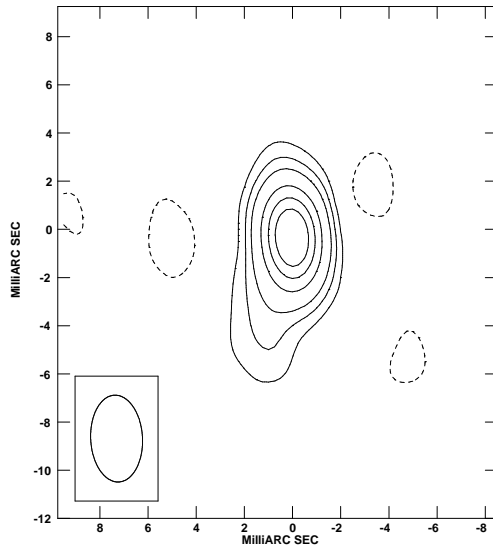


Fig. 13.— VLBA image at 5 GHz of 1502+26 (3C 310). Levs are: -0.15 0.15 0.3 0.5 1 1.5 2 mJy/beam

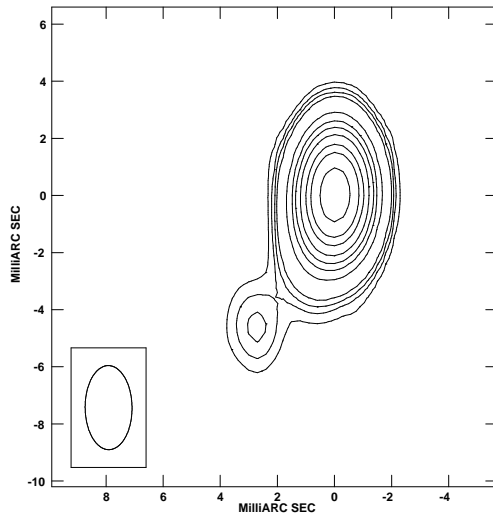


Fig. 14.— VLBA image at 5 GHz of 1521+28. Levs are: -0.3 0.3 0.5 0.7 1 3 5 7 10 15 20 30 mJy/beam.

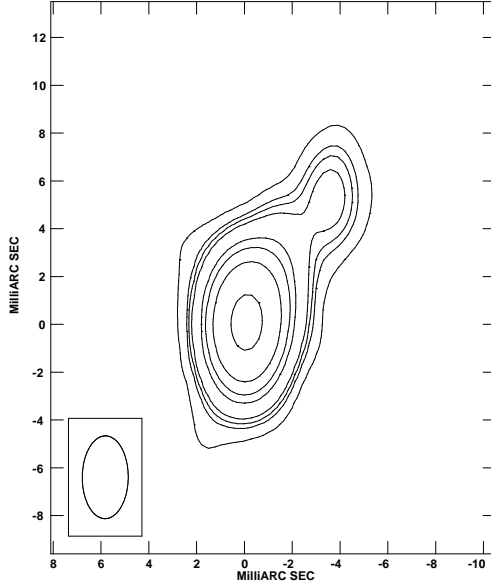


Fig. 15.— VLBA image at 5 GHz of 1553+24. Levs are: -0.2 0.2 0.5 0.7 1 3 5 10 30 mJy/beam

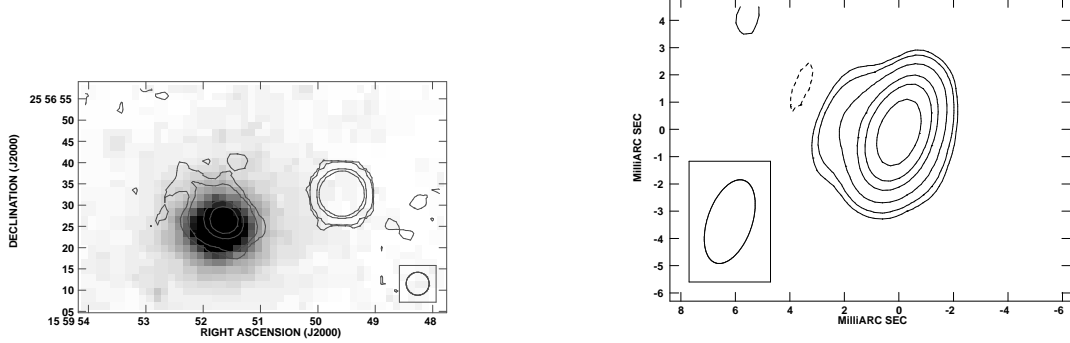


Fig. 16.— FIRST image of 1557+26 (IC4587) superimposed on the optical gray-scale image (left). Levs are: 0.3 0.7 5 10 mJy/beam, and VLBA image at 5 GHz of 1557+26 (right). Levs are: -0.4 0.3 0.5 1 2 3 5 mJy/beam.

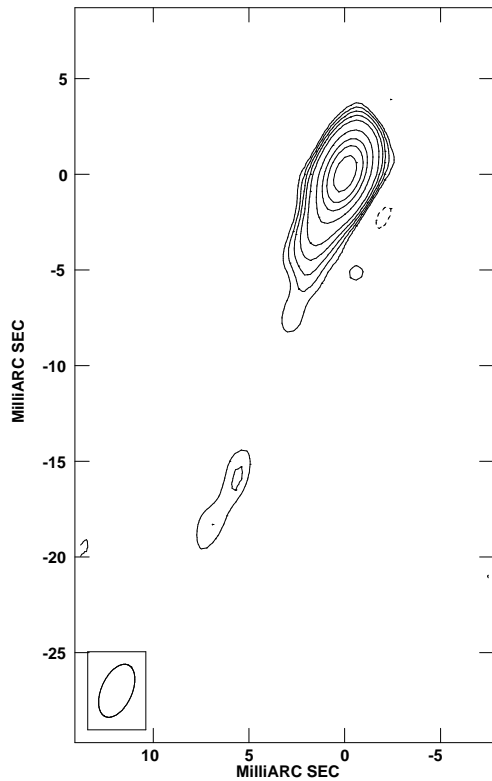


Fig. 17.— VLBA image at 5 GHz of 1621+38 (N6137). Levs are: -0.35 0.35 0.5 0.7 1 1.5 3 5 7 10 mJy/beam.

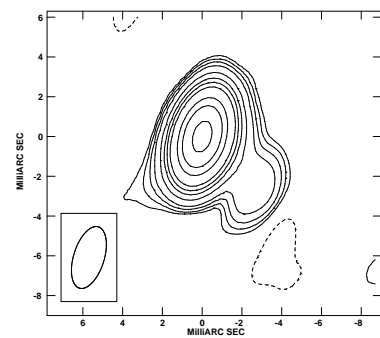


Fig. 18.— VLBA image at 5 GHz of 1658+30 (4C30.31). Levs are: -0.5 0.5 0.7 1 1.5 3 5 7 10 20 30 50 mJy/beam.

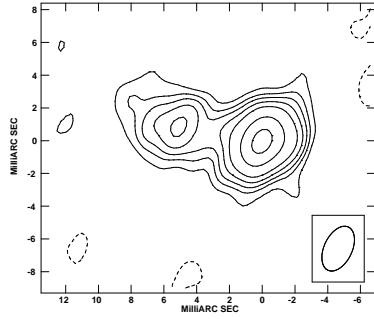


Fig. 19.— VLBA image at 5 GHz of 1827+32A. Levs are: $-0.3\ 0.3\ 0.5\ 0.7\ 1\ 1.5\ 3\ 5$ mJy/beam

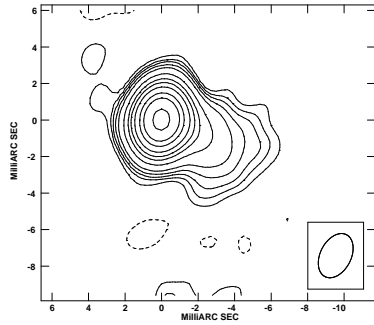


Fig. 20.— VLBA image at 5 GHz of 1842+45 (3C 388). Levs are: $-0.3\ 0.3\ 0.5\ 0.7\ 1\ 1.5\ 3\ 5\ 7\ 10\ 15\ 20\ 30$ mJy/beam.

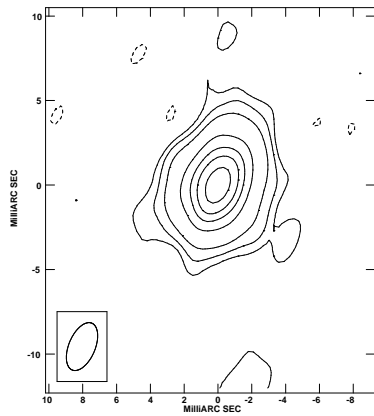


Fig. 21.— VLBA image at 5 GHz of 2229+39 (3C 449). Levs are: $-0.3\ 0.25\ 0.5\ 1\ 3\ 5\ 7\ 10$ mJy/beam.